Hippopede curves for modeling radial spin waves in an azimuthally graded magnonic landscape

D. Osuna Ruiz,* A. P. Hibbins, and F. Y. Ogrin
Department of Physics and Astronomy, University of Exeter, Exeter EX4 4QL, United Kingdom

(Received 25 June 2020; revised 25 August 2020; accepted 9 September 2020; published 23 September 2020)

We propose a mathematical model for describing radially propagating spin waves emitted from the core region in a magnetic patch with n vertices in a magnetic vortex state. The azimuthal anisotropic propagation of surface spin waves (SSWs) into the domain, and confined spin waves (or Winter's magnons) in domain walls, increases the complexity of the magnonic landscape. In order to understand the spin wave propagation in these systems, we first use an approach based on geometrical curves called "hippopedes"; however, it provides no insight into the underlying physics. Analytical models rely on generalized expressions from the dispersion relation of SSWs with an arbitrary angle between magnetization **M** and wave number **k**. The derived algebraic expression for the azimuthal dispersion is found to be equivalent to that of the hippopede curves. The fitting curves from the model yield a spin wave wavelength for any given azimuthal direction, number of patch vertices, and excitation frequency, showing a connection with fundamental physics of exchange-dominated surface spin waves. Analytical results show good agreement with micromagnetic simulations and can be easily extrapolated to any n-corner patch geometry.

DOI: 10.1103/PhysRevB.102.104430

I. INTRODUCTION

Due to their low loss and shorter wavelength compared to electromagnetic waves in free space, spin waves are a promising candidate for communicating information in micron and submicron scale magnonic circuits [1–3]. Spin wave spectra of magnetic circular nanodots have been studied intensively [4–7]. When an in-plane magnetic field excitation is applied to a vortex spin configuration, the lowest energy mode that can be excited is the gyration of the vortex core, which depends on the aspect ratio of the disk [8]. At higher frequencies, higher order gyrotropic modes [9,10] and a complete set of modes related to azimuthal and radial spin waves appear [4]. The latter types of spin waves are related to Damon-Eshbach modes where **k** is perpendicular to **M** in a vortex core configuration [11], and their spectra is strongly dependent on thickness and, more generally, on the physical geometry of the patch. Moreover, magnetization inhomogeneities such as vortex cores have attracted attention as spin waves emitters [12,13]. It is known that due to the confinement or the natural magnetic state of the sample, inhomogeneities of the internal magnetic field can be sources of spin waves due to a graded index in the magnonic landscape [14,15]. Spiraling spin waves found in vortex configurations have been explained as hybridization of stationary azimuthal spin waves and higher order gyrotropic modes, therefore showing no radial propagation [12,16,17].

Spin waves with spiral or circular wave fronts have been reported through micromagnetic simulations and experiments in simple elements such as circular disks or square patches [12,13,18]. In Ref. [12], the authors propose an analytical expression for the dispersion relation of radially propagating exchange-dominated spin waves from the core region, which are explained as laterally emitted spin waves from a first-order gyrotropic mode of the vortex core. Therefore, they manifest a "surface spin wave–like" (SSW-like) propagating behavior (since **M** is perpendicular to **k**).

In the past, a vast work on analytical modeling has dealt with magnetically nonsaturated structures presenting domain walls. Some examples are spin wave emission from Bloch domain walls [14], reflection and transmission across domain walls [19,20], or magnetic configuration in a transition between domain wall types [21]. These models help to provide insight into the dynamics and a tool for modeling spin wave phenomena in confined structures that show a more complex magnonic landscape than saturated dots. Thus far, we have not found in the literature a generalized mathematical model dedicated to the particular physics of the spiral or circular spin waves emitted from a point source in confined structures of more complex geometries than a circular disk, which are expected to considerably reshape the radial wave front [18].

Following on these studies, in this work we report on a model for the observed wave front of spin waves emitted from an almost point source (e.g., a vortex core) in any n-vertex patch, which implies the existence of domain walls, azimuthally distributed across the geometry. The final expression is derived from a generalization of the dispersion relation of surface waves for an arbitrary angle between magnetization **M** and wave number **k**. For $n > 2$, the patch adopts the form of a regular polygon; for $n = 2$ and $n = 1$, the model considers two or one single vertices. Finally, $n = 0$ implies a circular disk. The obtained curves from the model agree well with numerical results. In Sec. II we describe our models and the numerical method used for their validation. In Sec. III, we provide a comparison of both methods and their validation

*do278@exeter.ac.uk

through numerical simulations as well as a discussion of results. This model can help in the description of complex spin wave wave fronts in nonsaturated elements, which avoids running numerical simulations for particular shapes. Due to the attention that the experimentally observed short-wavelength radial spin waves have recently drawn, we believe this model is of interest to researchers, experimentalists mainly, working in the field of spin waves emitted from a point source.

II. NUMERICAL METHODS AND CALCULATIONS

In order to obtain an analytical solution for the spin wave wave front in a nonsaturated patch, we must make some initial approximations. This is due to the remarkable complexity of the magnetic configuration within the patch along the azimuthal direction, especially near magnetically inhomogeneous regions, which are determined by shape anisotropy and dipolar and exchange interactions solely. Thus, in our first approach we mathematically infer a general equation from numerical results and in our second approach, we extrapolate analytical results from a simpler case scenario to ours. Despite the apparent crudity of these extrapolations, both models show good agreement and therefore can be considered reliable for at least descriptive purposes. However, our second approach is more fundamental, and still, even after a crude generalization, it also shows very good agreement with micromagnetic results.

To obtain more insight into the dynamics and confirm the performance of our model, we performed a set of micromagnetic simulations using Mumax3 [22]. We simulated a circular microdisk with the typical material parameters of permalloy at room temperature with saturation magnetization $M_S = 8 \times 10^5$ A m^{-1}, exchange constant $A_{\text{ex}} = 1.3 \times 10^{-11}$ J m^{-1}, Curie temperature from a weighted average of iron and nickel $T_{\text{C}} = 270$ K, and Gilbert damping constant $\alpha = 0.008$. With these parameters, the single circular disk was simulated in a hexahedral grid. Shapes with diameter d of 900 nm and thickness t of 80 nm were simulated. The grid was discretized in the x, y, z space into $512 \times 512 \times 16$ cells. The cell size along x and y was 3.9 nm, while the cell size along z was fixed to 4 nm. The cell size along three dimensions is always kept smaller than the exchange length of permalloy (5.3 nm). The number of cells was chosen to be powers of 2 for the sake of computational efficiency. We also set a "smooth edges" condition with value 8 [22]. A key point in micromagnetic simulations is to achieve a stable equilibrium magnetization state. We first set a vortex state with polarity and chirality numbers of $(1, -1)$ and then executed the simulation with a high damping ($\alpha = 1$) to relax the magnetization until the maximum torque$/\gamma$ ("maxtorque" parameter in Mumax3) reached 10^{-7} T indicating convergence and the achievement of a magnetization equilibrium state. The typical time to achieve the equilibrium state was 100 ns. Once the ground state was obtained, damping was set back to $\alpha = 0.008$ and the relaxation process repeated. The microdisk spin configuration was recorded as the ground state of the sample and then used for the simulations with the dynamic activation.

For analyzing time evolution of the magnetic signal, we apply a continuous wave excitation at the core region with a magnetic field B_0 at a specific frequency f_0,

$$B_0(t) = A_0 \sin(2\pi f_0 t), \tag{1}$$

where f_0 is the microwave excitation frequency and pulse amplitude $A_0 = 0.3$ mT. This is small enough to remain in the linear excitation regime and avoid any changes to the equilibrium state. A sampling period of $T_s = 25$ ps was used, recording up to 200 simulated samples in space and time, only after the steady state is reached.

In the next sections we describe the proposed models and their derivations. Finally, validations for each of them through numerical simulations are shown.

A. First approach

For this study, we mathematically infer a fitting model from numerical results on the first obtained shapes when $n = 0, 1, 2, 3, 4, \ldots$ and so on. We then generalize it to any n-vertex patch. For the case of $n = 1$ we take an internal angle assumed to be $\pi/3$ and only one domain wall is present, the patch resembling a "teardrop" shape. For $n = 2$ we make a similar assumption, and the patch resembles a "double-teardrop" shape. For larger values of n, the internal angles of the vertices are the internal angles of the regular polygons, defined as $2\pi(n-2)/n$. Of course, for $n = 0$ we have a circle. The vertices are distributed around the shape, separated by $2\pi/n$ radians, and the resulting domain walls spaced by π/n.

Regarding magnetic configuration in equilibrium after a relaxation process, and assuming a centered vortex core, n triangular domains and n domain walls will form in the patch. In contrast to the circular dot, the azimuthally distributed domain walls will distort the wave front of the propagating spin wave from the core region, introducing an azimuthal dependence (or equivalently, n dependence) to the wavelength of the radial wave $[\lambda(\theta)]$. Also, two known values for the spin wave wavelength can be analytically deduced for any n-corner patch: the characteristic wavelength of an exchange-dominated surface spin wave (λ_{SSW}), when $\mathbf{k}$ is perpendicular to $\mathbf{M}$ (that is, when the spin wave propagates into the domain), and the characteristic wavelength of the confined spin wave along the domain wall (λ_{WM}), also known as Winter's magnon [23]. Figure 1 shows the characteristic dispersion relations for the laterally emitted spin wave from the vortex core from Ref. [12] (blue curve) and the exchange-dominated Winter's magnon in an ideal 180° Bloch wall [24] (orange curve). It is worth noting that in an n-vertex patch, the formed domain walls will be of the angle of the vertex. For example, in a square ($n = 4$), this is an angle of 90° (see the top-right inset in Fig. 1). Micromagnetic simulations (not shown here) show that the expected wave number is reduced with respect to the 180° Bloch wall, due to the shape anisotropy of the sharp corner. This latter study is not in the scope of this article (although it will be addressed in a future work) and the effects of an intermediate domain wall are not included in our model. For practical purposes, we obtain k_{WM} from the dispersion relation of an ideal 180° Bloch wall (see orange curve in Fig. 1). For excitation frequencies at which both modes coexist, the wave numbers (or wavelengths) that fall in the gray area, delimited by k_{SSW} and k_{WM}, can relate to the azimuthally dependent wavelength of the radial spin wave in the patch.

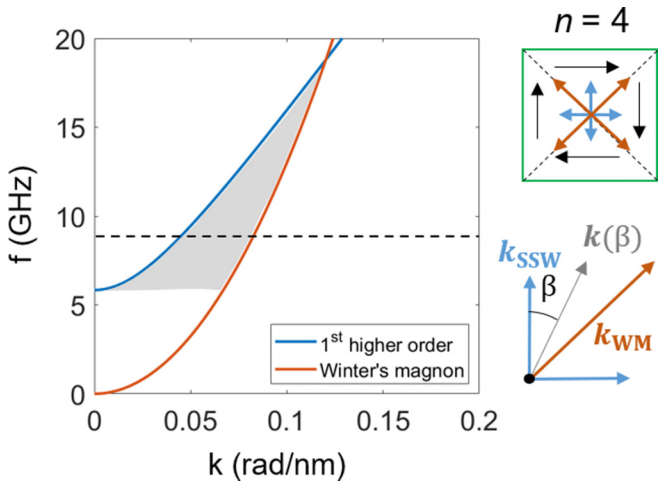

FIG. 1. Dispersion relations for the laterally emitted spin wave from a first higher order dynamical core, see Ref. [12], and a Winter's magnon (WM), for the material parameters indicated in Sec. II, as limiting cases. Dashed horizontal line indicates an excitation frequency of 8.8 GHz. Gray area highlights the expected magnitudes for intermediate wave vectors (see bottom-right inset) between the two limiting cases, when being simultaneously excited. Insets: Color arrows show the wave vectors for the laterally emitted spin wave (in a SSW configuration) and the Winter's magnon, which are assumed $k_{\mathrm{WM}} \approx 2k_{\mathrm{SSW}}$ for the excitation frequency of 8.8 GHz (length of the vectors represent their magnitudes). Black arrows show the orientation of magnetization in the domains. Bottom inset shows a simplified schematic of the angular distribution of wave vectors at the top-right corner of a square patch ($n = 4$). Gray arrow is an intermediate case for the spin wave wave vector between the limiting cases, from which an angular dependence can be inferred.

The proposed model is based on the mathematical expressions of a family of curves known as "hippopedes." Since the polar representation of these curves allows a smooth azimuthal transition from a certain wavelength (maximal) to another finite value (minimal), these curves can be used here as a generalization of the problem scenario. By applying these expressions to the particular scenario, i.e., a magnetic patch with regularly distributed vertices and domain walls, a simple expression for the spin wave wavelength can be obtained. From a conic canonical equation with geometrical parameters a and b, see [25] for a more detailed description, then the generic equation of the resulting hippopede in polar coordinates is

$$f(\theta) = 2\sqrt{b}\sqrt{a - b\sin^2\left(\theta\frac{n}{2} + \phi_0\right)}, \qquad (2)$$

where the phase parameter ϕ_0 sets an initial rotation angle for the patch. For $n = 2$ and $b = 2a$, Eq. (2) leads to a special case known as Bernoulli's lemniscate. In fact, a whole family of lemniscates can be obtained from the hippopedes if $b > a$. More information on the hippopede curves can be found in the Supplemental Material [25]. The hippopedes when $b < a$, known as Booth's ovals, allow a transition from a finite-wavelength maximum value (λ_{SSW}) to another nonzero minimum value (λ_{WM}); see Fig. 2(b). The particular values of the geometrical parameters a and b can be found from the

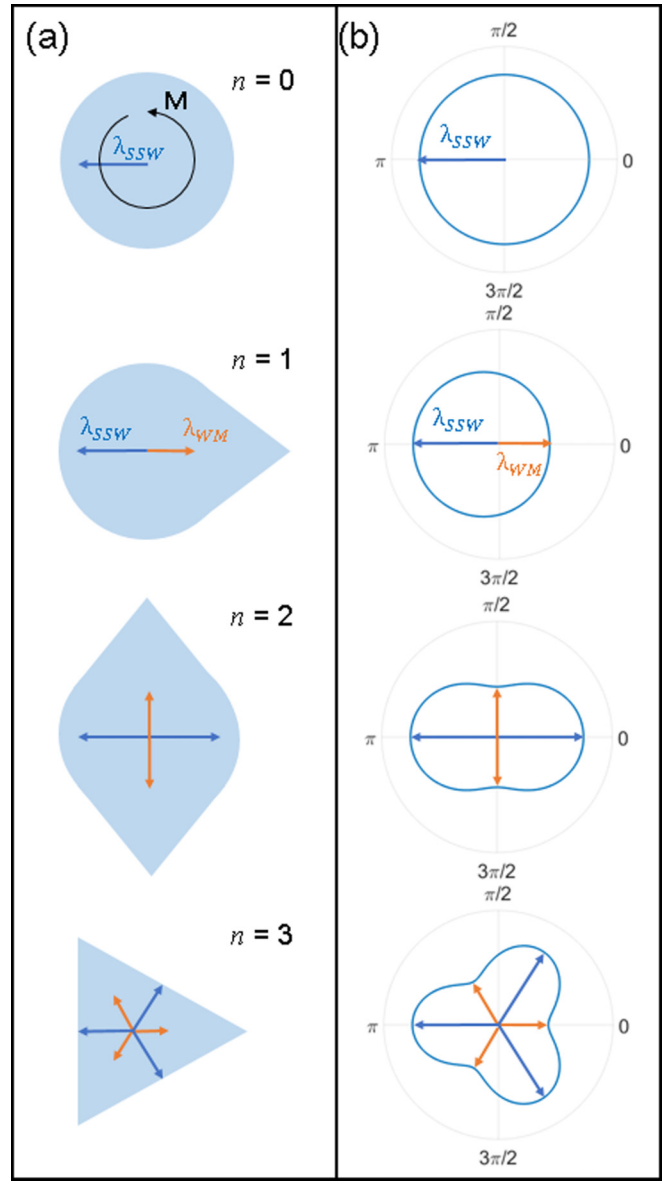

FIG. 2. (a) Schematic of various magnetic patches depending of the number of vertices n with magnetization around the core (solid black line). Domain walls bisect the sharp corners. (b) Polar representation of Eq. (2) showing the azimuthal variation of wavelength within the shape, with the appropriate rotation of the patch (ϕ_0) so the equation describes correctly the shape of the patch. Minimum and maximum radial amplitudes are assumed $\lambda_{\mathrm{SSW}} = 2\lambda_{\mathrm{WM}}$ (length of the vectors represent their magnitudes). In terms of the hippopedes parameters a and b, this means a ratio of $b/a = 0.75$.

hippopede general equation particularized to the wavelength limiting conditions of a maximum λ_{SSW} at every $2\pi/n$ angle and a minimum λ_{WM} at every $2\pi/n + \pi/n$ angle. An initial rotation angle of $\phi_0 = 0$ is assumed. The ratio b/a is found to be equal to $1 - \lambda_{\mathrm{WM}}^2/\lambda_{\mathrm{SSW}}^2$. In the range of frequencies under study, $\lambda_{\mathrm{SSW}} > \lambda_{\mathrm{WM}}$ is satisfied, so this implies that we can model our system with hippopede curves where $b < a$. The initial phase rotation ϕ_0 in Fig. 2(b) (and hereafter) is chosen so it properly coincides with the numerically modeled patch. Therefore, a more complete expression for our

model is

$$\lambda(\theta, n) = \lambda_{\mathrm{SSW}} \sqrt{1 - \left(1 - \frac{\lambda_{\mathrm{WM}}^2}{\lambda_{\mathrm{SSW}}^2}\right) \sin^2\left(\theta \frac{n}{2} + \phi_0\right)}. \quad (3)$$

Figure 2(b) shows a collection of curves from Eq. (3) for different number of vertices n. Following from the magnetic configuration of the patch in the vortex state and assuming for example $\lambda_{\mathrm{SSW}} = 2\lambda_{\mathrm{WM}}$, which yields a ratio $b/a = 0.75$ ($b < a$), results qualitatively show an azimuthal changing wavelength around the center of the shape according to a hippopede curve. In Sec. II B, we derive a more generalized expression that yields a connection with the fundamental physics.

B. Second approach

In this case, we start from the analytical expression of the dispersion relation of surface spin waves given an arbitrary angle α between **M** and **k**. Damon and Eshbach [11] found a generalized expression for the dispersion relation of surface spin waves in a semi-infinite stripe for arbitrary angles α and β, α being the angle between the ferromagnetic planar body surface and effective field H_i, and β the angle between the orthogonal direction of that effective field and wave number **k**. Extended to the exchange regime, it can be expressed as

$$\omega = \frac{\gamma H_i}{2\cos\alpha\cos\beta} + \frac{\gamma B_i}{2}\cos\alpha\cos\beta + \omega_M \lambda_{\mathrm{ex}} k^2. \quad (4)$$

In Ref. [11], the original expression is derived for magnetostatic spin waves in a semi-infinite stripe. It should be noted that our problem scenario, although being a finite sample, can still be regarded equivalent due to the short wavelength of the spin wave modes under study [11]. In Ref. [11], the expression shows a continuous variation of the spin wave wavelength as angle increases, toward the limiting scenario of a backward volume spin wave (BVSW) configuration. It is worth noting that in our problem scenario, that limiting case would not be the BVSW dispersion relation but the Winter's magnon (see Fig. 1). Also, in nonsaturated samples, Eq. (4) can be reduced by specifying only in-plane magnetization ($\alpha = 0$), assuming that the internal field in the magnetic domain is $\mathbf{H}_i = -\mathbf{M}_S$ (therefore, $H_i = M_S$ and $\mathbf{B}_i = 0$) in absence of an external biasing field. For $\beta = 0$, **k** is perpendicular to **M** (**k** $\perp$ **M**) and therefore $\lambda = \lambda_{\mathrm{SSW}}$ (see inset in Fig. 1). Hence, for a specific excitation frequency $\omega = \omega_0$ we can rewrite Eq. (4) in terms of a variable wavelength ($\lambda = 2\pi/k$) in the azimuthal direction β (as defined in Fig. 1 and in Ref. [11]) as (a step-by-step derivation is shown in the Supplemental Material [25])

$$\lambda(\beta) = \lambda_{\mathrm{SSW}} \sqrt{\frac{(1-p)\cos\beta}{\cos\beta - p}}, \quad (5)$$

where $\beta = \theta$, with θ being the azimuthal direction as defined in Eq. (2) and Eq. (3) that coincides with the angle β, setting the reference for an azimuthal dependence of **k** at $\theta = 0$, and $p = \omega_M/2\omega_0$, where $\omega_M = \gamma M_S$. We obtain a classical surface spin wave dispersion behavior from Eq. (5) when $\theta = 0$. In Eq. (2), the initial arbitrary rotation phase of the patch can be conveniently chosen as $\phi_0 = \pi/2$ so a surface spin wave wavelength can be effectively obtained for $\theta = 0$, as a reference point. This implies we can substitute $\sin(\theta + \phi_0) \to \cos(\theta)$ in Eq. (2), which keeps the reference $\lambda(0) = \lambda_{\mathrm{SSW}}$ consistent with Eq. (5). Equation (5) implies a decreasing wavelength as the angle θ (or equivalently, β) increases. For a flux closure magnetization in the patch, the reference angle coincides with the direction of propagation into a first magnetic domain.

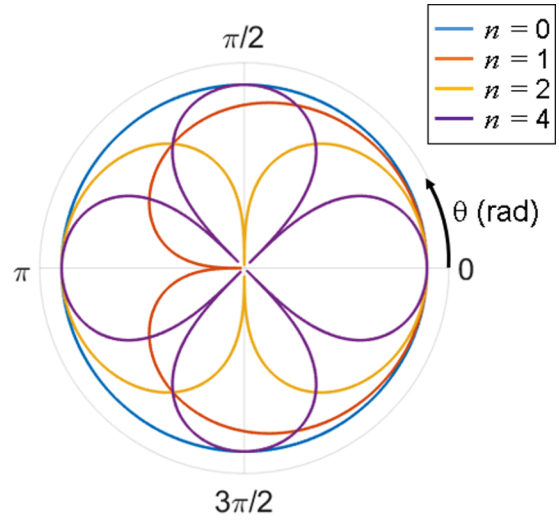

FIG. 3. Collection of curves from Eq. (5) for $n = 0$, 1, 2, and 4. Curves for $n = 3$ and higher orders ($n > 4$) can be easily inferred. Physically nonrealizable zeros are placed at every π/n angle.

In the model, parameter $p = \omega_M/2\omega_0$ yields a connection between the observed radial wave front in simulations and the magnetic properties of the material but sets an upper frequency bound for the model, which is not physically meaningful. The model from Eq. (5) yields imaginary values for $\cos(\theta) < p \leqslant 1$ and therefore, it would only be applicable for $\omega_0 < \omega_M/2$ and for certain azimuthal directions. Equation (5) would still be applicable as a model for the scenario of a magnetic patch for small deviations of θ from 0, although it does not apply when $\theta \to \pi/2$, where the backward volume spin wave propagates instead of surface spin waves according to Ref. [11].

Also, this preliminary model assumes in-plane magnetization for all azimuthal directions, so it still does not take into account effects of magnetic inhomogeneities, i.e., the domain walls. Figure 3 shows a collection of curves from Eq. (5) illustrating a periodic effect when an n number of corners is included ($\theta \to n\theta/2$). In Fig. 3, only the rightmost lobe would be strictly represented by Eq. (5), i.e., for values of $-\pi/n < \theta < \pi/n$ and $n > 0$.

As stated above, imaginary values and zeros of Eq. (5) due to the frequency dependence and geometry are not physically meaningful in our scenario. This is due to the imposed lower frequency gap for the ferromagnetic resonance in the disk and the presence of domain walls, respectively. To include these phenomena and avoid the zeros in the model, Eq. (5) has to be generalized with the undefined parameter σ and rescaling factor ϵ so the expression is extended as

$$\lambda(\theta, n) = \epsilon\, \lambda_{\mathrm{SSW}} \sqrt{\sigma + \frac{(1-p)\cos\left(n\frac{\theta}{2}\right)}{\cos\left(n\frac{\theta}{2}\right) - p}}. \quad (6)$$

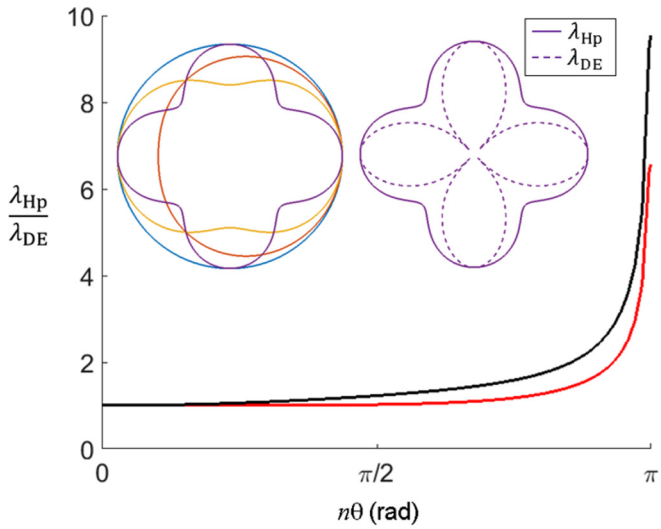

FIG. 4. Ratio (black solid curve) between wavelengths from the dispersion relation from [11] (λ_{DE}) and the extended model linked to the hippopedes (λ_{Hp}) for $p \approx 1.75$ showing good agreement, and practically no deviation from unity at any angle apart from the domain wall region for $p \approx 10.75 \gg 1$ (red solid curve). Left inset: Normalized results from Eq. (7) adding azimuthal periodicity for a number of corners $n = 0$ (blue), $n = 1$ (red), $n = 2$ (yellow), and $n = 4$ (purple). Right inset: Comparison of the normalized results from Eq. (7) (solid purple curve) and Eq. (5) (dashed purple curve) for $n = 4$ and $p \approx 1.75$.

In an n-corner patch, the spin wave shows a wavelength of λ_{SSW} at every $2\pi/n$ angle and of λ_{WM} at every π/n angle. These limiting conditions allow us to find the values of parameters ϵ and σ. The values for ϵ and σ are found to be $\epsilon = (\sqrt{\lambda_{SSW}^2 - \lambda_{WM}^2})/\lambda_{SSW}$ and $\sigma = \lambda_{WM}^2/(\lambda_{SSW}^2 - \lambda_{WM}^2)$, which, simplified for $\lambda_{WM} = 0$, lead to the equation from Ref. [11]. Due to the azimuthal periodicity every π/n (in contrast to the scenario described in Ref. [11]), the cosine terms in Eq. (6) must only take positive values. Also, since taking their absolute value would yield a nondifferentiable function at the angle where the domain wall is encountered, the cosine terms are replaced by their squared values. Assuming $\lambda_{WM} \neq 0$ and after algebraic transformations, the modified equation is

$$\lambda(\theta, n) = \lambda_{WM}\sqrt{1-\left(1-\frac{\lambda_{SSW}^2}{\lambda_{WM}^2}\right)\frac{(1-p)}{\cos^2\left(n\frac{\theta}{2}\right)-p}\cos^2\left(n\frac{\theta}{2}\right)}, \tag{7}$$

where $p = \omega_M/2\omega_0$. Our key result is obtained if $p \gg 1$ and therefore $(1-p)/[\cos^2(n\theta/2) - p] \approx 1$. Then, the resultant equation is indeed the hippopede curve equation (assumed $\phi_0 = \pi/2n$, so the directions for λ_{WM} and λ_{SSW} are exchanged) described in Sec. II A, which explains the good fitting to these curves at low frequencies ($\omega_0 \ll \omega_M/2$). Therefore, the azimuthal change of wavelength for a spin wave emitted from the core in an n-corner magnetic patch in the vortex configuration is fully described by hippopede curves.

Figure 4 (left inset) shows a collection of curves obtained from Eq. (7) normalized to λ_{SSW}, assuming $\lambda_{SSW} = 2\lambda_{WM}$ (see Fig. 1). In the right inset, a particular case for $n = 4$ is shown in comparison with the respective solution from Eq. (5) and the relative error between both equations for all angles between 0 and π/n, normalized to the number of vertices n for a value $p \approx 1.75$ (black solid curve), obtained from assuming $\omega_0/2\pi = 8.8$ GHz and from Permalloy material properties, $\omega_M/2\pi \approx 27$ GHz. For a large enough value of p, assumed to be about six times larger ($p \approx 10.75$), and therefore $p \gg 1$, results show indeed a minimal difference from the hippopede curves (red solid curve), almost negligible away from the domain wall regions. The proposed model, as an extension of Eq. (5), avoids the azimuthal zeros and shows a minimal difference from the values from the exchange-dominated surface spin wave dispersion. Therefore, Eq. (7) is a suitable model, derived as a generalization from Eq. (5). In Sec. III, we provide numerical evidence of its reliability.

III. NUMERICAL RESULTS AND DISCUSSION

In this section we compare the models previously described to numerical micromagnetic simulations in order to validate them. Radial spin waves with a spiral profile from the core region can also propagate, when the excitation signal is applied in-plane of the patch [13]. This effect can be added to the model in terms of a normalized azimuthal factor that creates a counterclockwise spiralling effect as observed in the simulated wave fronts $[\lambda(\theta) \rightarrow \frac{\theta}{2\pi}\lambda(\theta)]$. In micromagnetic simulations, a continuous out-of-plane wave excitation of frequency $\omega_0/2\pi = 8.8$ GHz is applied to the core region. The excitation frequency is chosen so the radial spin wave shows a clear wave front for the given dimensions and material of the magnetic patch [18]). From Fig. 1 (and numerical results from [18]), the wavelengths of the spin wave into the domain and the confined mode are chosen as $\lambda_{SSW} = 135$ nm and $\lambda_{WM} = 89$ nm. The condition $\lambda_{SSW} > \lambda_{WM}$ is satisfied by applying an oscillating magnetic field in the GHz range. We need to address that the main objective is to test the relative change between these two wavelengths, regardless of their absolute values. Figure 5(a) shows snapshots of the dynamic out-of-plane magnetization from micromagnetic simulations of two different shapes, a double-teardrop shape (two vertices) and a square (four vertices). Their respective **k**-space maps from each image are shown on the right, where the white arrows indicate the propagation of the main modes, surface spin waves and Winter's magnons. The images are interpolated for clarity. Before performing a spatial fast Fourier transform, a Hamming window of 256 points is applied to the data set to avoid image artifacts due to reflections at the edges and spurious high-frequency values.

Values of wavelength are extracted from the simulated **k**-space images at angles from 0 rad to $\pi/2$ in the teardrop shape and from 0 rad to $\pi/4$ in the square in steps of $\pi/16$. The error bars are found after interpolation, yielding an error in wavelength of approximately 8 nm. The change in wavelength given by the model shows very good agreement with numerical results and follows the predicted trend. The analytical results can easily be extrapolated to any n-corner shape. Taking this into account, we can confidently say that the proposed model describes the spin wave wave front of an

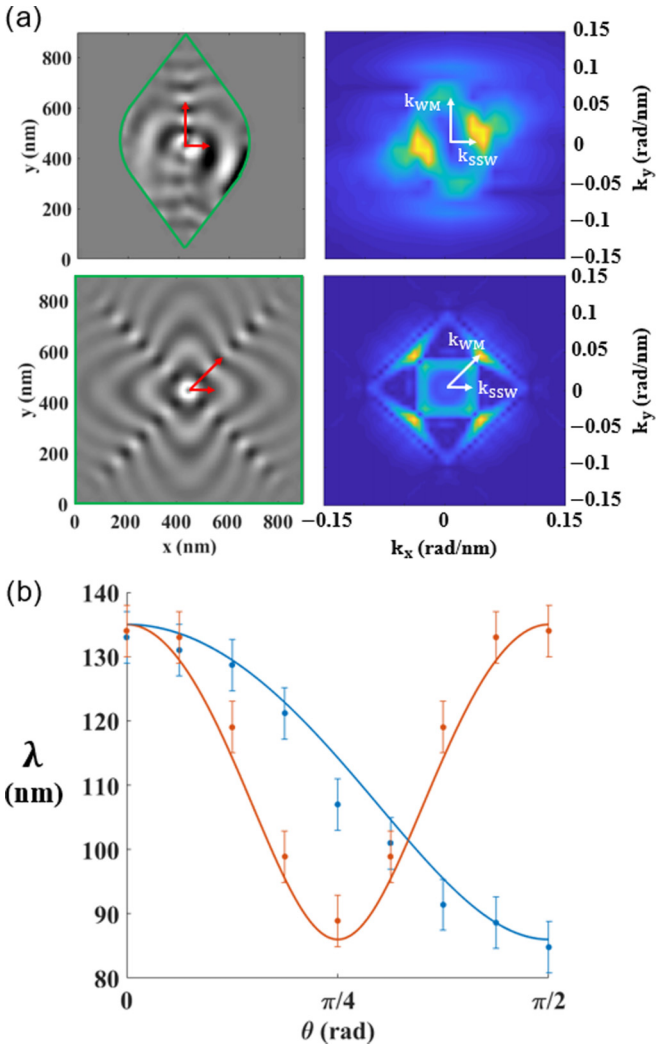

FIG. 5. (a) Left: Snapshots of numerical results for a double-teardrop shape ($n = 2$) and a square ($n = 4$). Red arrows indicate the direction of propagation of the two main modes (surface spin wave and Winter's magnon). Right: **k** space of the snapshots where the wave number profile (inverse of the wavelength profile) is shown. Results are interpolated to 5 extra points between data points for clarity. White arrows show the direction of propagation of the main modes. (b) Comparison of the maximum values of $\lambda = 2\pi/k$ found in (a) for the double-teardrop shape (blue) and the square (orange) with the results from Eq. (6) where $\lambda_{SSW} = 135$ nm and $\lambda_{WM} = 89$ nm found from numerical results at $\omega_0/2\pi = 8.8$ GHz and $p \approx 1.75$. Error bars are found after the interpolation process, which introduces a measured error of approximately 8 nm.

emitted spin wave from the core in any n-corner shape with accuracy.

Finally, in any n-corner shape presenting angular periodicity, the azimuthal transition from a surface spin wave of wavelength λ_1 into that of a confined mode along a domain wall $\lambda_2 < \lambda_1$ is of the form of a hippopede curve or, more generalized,

$$\lambda(\lambda_1, \lambda_2, \theta, n) = \lambda_1 f(\lambda_1, \lambda_2, \theta, n)\sqrt{1 - g(\lambda_1, \lambda_2)\cos^2\left(\theta\frac{n}{2}\right)}, \quad (8)$$

where functions f and g are generic functions of the indicated magnitudes.

As a suggested improvement to the model, a radial dependence could be included into Eq. (7). The radial dependence should consider that, as n increases, the domain walls will merge closer to the core region, which implies no azimuthal gradient and the wave front profile will be that of a disk (equivalent to $n = 0$) under a critical effective radius.

The hippopede curves are obtained from Eq. (7) under the condition $p \gg 1$. It is worth noting that the condition $\sqrt{2}\lambda_{WM} > \lambda_{SSW} > \lambda_{WM}$, which implies a "hippopede wave front" with geometrical parameters $b < a$, is not necessarily satisfied for all values of $\lambda(\theta)$ at every ω_0, as explained before. Although the extended model avoids an upper frequency bound, there is a lower frequency bound from which only spin waves will be radiated into the domains from the core due to the nonzero internal field there. In contrast, a gapless mode can propagate in the domain walls [24]. As ω_0 increases, at the limit when $\lambda_{SSW} \approx \lambda_{WM}$, the wave front tends to a circular profile, as explained elsewhere [18] and as Eq. (7) consistently predicts. This frequency dependence is already implicit in the model in parameter $p = \omega_M/2\omega_0$. At high frequencies where $\omega_0 \approx \omega_M/2$ and therefore $p \approx 1$ (so $p \gg 1$ is not hold), assuming $\lambda_{SSW} \approx \lambda_{WM}$, Eq. (7) effectively yields a wavelength of $\lambda(\theta, n) = \lambda_{SSW}$, that is, a circular wave front, which is confirmed by micromagnetic simulations and elsewhere.

At even higher frequencies ($\omega_0 \gg \omega_M$), $p \ll 1$ and therefore $(1 - p)/[\cos^2(n\theta/2) - p] \approx 1/\cos^2(n\theta/2)$, Eq. (7) leads again to $\lambda(\theta, n) = \lambda_{SSW}$, regardless of λ_{SSW} and λ_{WM} values. This implies that Eq. (7) is still a valid model even for $p \approx 1$ or $p \ll 1$, or in other words, it does not show an upper frequency bound for radial waves. This is consistent with the physical scenario to describe and previous work on radially propagating spin waves.

Previous work on exchange-dominated radial spin waves has predominantly dealt with direct observation or experimental detection, as referred to in Sec. I. We believe that our results may help in obtaining further information on these spin waves such as an expression for a spatially dependent wavelength, potential detection of magnetic inhomogeneities in magnetic films of various geometries, or characterization of the material properties, when used, for example, as a fitting tool. We would also like to highlight the applicability of these mathematical curves itself. We believe that, in addition to their known applications in mechanical linkages (see Supplemental Material [25]), the work proposed here is another interesting use of these curves for modeling in physics and, in particular, a novelty in magnetism.

IV. SUMMARY

We have used geometrical expressions to successfully model propagating spin waves from the vortex core region in n-corner elements in a magnetic flux closure configuration where domain walls are present. The proposed models are validated and all show very good agreement with numerical results. The equations can be generalized to any n-corner shape, including nonregular shapes such as a teardrop shape (one corner) and a double-teardrop shape (two corners). A

first model is based on a special case of the hippopede curves, known as Booth's ovals, since they allow smooth transitions between two known wavelength values. A more exact model is obtained straight from generalizing the fundamental equation of surface spin wave dispersion, which can be retrieved by setting $\lambda_{WM} = 0$. This more compact model describes the spin wave wave front accurately at positions far from the core and, especially, close to the inhomogeneous areas (i.e., domain walls). Interestingly, through algebraic transformations, the final equation of the model (where $\lambda_{WM} \neq 0$ and $p \gg 1$) is identical to the equation of the hippopede curve. The result connects the mathematical model with the physical parameters of the material and proves the hippopede curves as the most accurate mathematical description of the transition between one wavelength and the other. Reciprocally, the magnetic properties of the material (through λ_{WM} and λ_{SSW}) can be retrieved from the geometrical parameters of the plotted Hippopede curve (a and b). Given the frequency of the oscillating field ω_0, parameter p and therefore ω_M and M_S can also be retrieved.

The model from Eq. (7) also takes into account the frequency dependence of the oscillating field. At lower frequencies, the model yields hippopede curves for the spin-wave wave-front profile. At higher frequencies, it effectively leads to circular wave fronts, as expected from numerical results.

The models can also be applied on spiral wave fronts, although they are originally defined for ''in-phase" wave fronts, which makes them suitable for also describing circular/nonspiraling wave fronts. For modeling spiral wave fronts, the equation must be modified accordingly by simply introducing a normalized spiraling effect factor. We hope these results help to better understand the propagating features of spin waves in confined structures, more especially those emitted from quasipunctual sources, and how to control their dynamical properties.

All data created during this research are openly available from the University of Exeter's institutional repository [26].

ACKNOWLEDGMENTS

This work was supported by Engineering and Physical Sciences Research Council (EPSRC) and the Centre of Doctoral Training (CDT) Grant No. EP/L015331/1 in Metamaterials, University of Exeter.

[1] V. V. Kruglyak, S. O. Demokritov, and D. Grundler, J. Phys. D **43**, 264001 (2010).
[2] A. D. Karenowska, A. V. Chumak, A. A. Serga, and B. Hillebrands, in *Handbook of Spintronics*, edited by Y. Xu, D. D. Awschalom, and J. Nitta (Springer Netherlands, Dordrecht, 2016), pp. 1505–1549.
[3] A. Hoffmann and S. D. Bader, Phys. Rev. Appl. **4**, 047001 (2015).
[4] B. Taurel, T. Valet, V. V. Naletov, N. Vukadinovic, G. de Loubens, and O. Klein, Phys. Rev. B **93**, 184427 (2016).
[5] G. N. Kakazei, P. E. Wigen, K. Y. Guslienko, V. Novosad, A. N. Slavin, V. O. Golub, N. A. Lesnik, and Y. Otani, Appl. Phys. Lett. **85**, 443 (2004).
[6] M. Bailleul, R. Höllinger, K. Perzlmaier, and C. Fermon, Phys. Rev. B **76**, 224401 (2007).
[7] M. Bailleul, R. Höllinger, and C. Fermon, Phys. Rev. B **73**, 104424 (2006).
[8] V. Novosad, K. Yu. Guslienko, H. Shima, Y. Otani, S. G. Kim, K. Fukamichi, N. Kikuchi, O. Kitakami, and Y. Shimada, Phys. Rev. B **65**, 060402 (2002).
[9] J. Ding, G. N Kakazei, X. Liu, K. Guslienko, and A. Adeyeye, Sci. Rep. **4**, 4796 (2014).
[10] K. Y. Guslienko, G. N. Kakazei, J. Ding, X. M. Liu, and A. O. Adeyeye, Sci. Rep. **5**, 13881 (2015).
[11] J. R. Eshbach and R. W. Damon, Phys. Rev. **118**, 1208 (1960).
[12] G. Dieterle, J. Förster, H. Stoll, A. S. Semisalova, S. Finizio, A. Gangwar, M. Weigand, M. Noske, M. Fähnle, I. Bykova, J. Gräfe, D. A. Bozhko, H. Y. Musiienko-Shmarova, V. Tiberkevich, A. N. Slavin, C. H. Back, J. Raabe, G. Schütz, and S. Wintz, Phys. Rev. Lett. **122**, 117202 (2019).
[13] C. S. Davies, A. Francis, A. V. Sadovnikov, S. V. Chertopalov, M. T. Bryan, S. V. Grishin, D. A. Allwood, Y. P. Sharaevskii, S. A. Nikitov, and V. V. Kruglyak, Phys. Rev. B **92**, 020408(R) (2015).
[14] N. J. Whitehead, S. A. R. Horsley, T. G. Philbin, A. N. Kuchko, and V. V. Kruglyak, Phys. Rev. B **96**, 064415 (2017).
[15] F. B. Mushenok, R. Dost, C. S. Davies, D. A. Allwood, B. J. Inkson, G. Hrkac, and V. V. Kruglyak, Appl. Phys. Lett. **111**, 042404 (2017).
[16] H. Stoll, M. Noske, M. Weigand, K. Richter, B. Krüger, R. M. Reeve, M. Hänze, C. F. Adolff, F.-U. Stein, G. Meier, M. Kläui, and G. Schütz, Front. Phys. **3**, 26 (2015).
[17] M. Kammerer, M. Weigand, M. Curcic, M. Noske, M. Sproll, A. Vansteenkiste, B. V. Waeyenberge, H. Stoll, G. Woltersdorf, C. H. Back, and G. Schuetz, Nat. Commun. **2**, 279 (2011).
[18] D. Osuna Ruiz, E. B. Parra, N. Bukin, M. Heath, A. Lara, F. G. Aliev, A. P. Hibbins, and F. Y. Ogrin, Phys. Rev. B **100**, 214437 (2019).
[19] L.-J. Chang, Y.-F. Liu, M.-Y. Kao, L.-Z. Tsai, J.-Z. Liang, and S.-F. Lee, Sci. Rep. **8**, 3910 (2018).
[20] X.-g. Wang, G.-h. Guo, G.-f. Zhang, Y.-z. Nie, and Q.-l. Xia, Appl. Phys. Lett. **102**, 132401 (2013).
[21] M. D. DeJong and K. L. Livesey, Phys. Rev. B **92**, 214420 (2015).
[22] A. Vansteenkiste, J. Leliaert, M. Dvornik, M. Helsen, F. Garcia-Sanchez, and B. Van Waeyenberge, AIP Adv. **4**, 107133 (2014).
[23] J. M. Winter, Phys. Rev. **124**, 452 (1961).
[24] F. Garcia-Sanchez, P. Borys, R. Soucaille, J.-P. Adam, R. L. Stamps, and J.-V. Kim, Phys. Rev. Lett. **114**, 247206 (2015).
[25] See Supplemental Material at http://link.aps.org/supplemental/10.1103/PhysRevB.102.104430 for a more detailed mathematical description of the hippopede curves and a derivation of Eq. (5).
[26] See https://ore.exeter.ac.uk/repository.